INL/CON-26-91776-Revision-0

Enabling Grid-Forming Control Under Unbalanced Conditions

December 2025

Yemi Ojo, Soumyadeep Nag, Temitayo Olayemi Olowu

Changing the World's Energy Future

INL is a U.S. Department of Energy National Laboratory operated by Battelle Energy Alliance, LLC

DISCLAIMER

This information was prepared as an account of work sponsored by an agency of the U.S. Government. Neither the U.S. Government nor any agency thereof, nor any of their employees, makes any warranty, expressed or implied, or assumes any legal liability or responsibility for the accuracy, completeness, or usefulness, of any information, apparatus, product, or process disclosed, or represents that its use would not infringe privately owned rights. References herein to any specific commercial product, process, or service by trade name, trade mark, manufacturer, or otherwise, does not necessarily constitute or imply its endorsement, recommendation, or favoring by the U.S. Government or any agency thereof. The views and opinions of authors expressed herein do not necessarily state or reflect those of the U.S. Government or any agency thereof.

INL/CON-26-91776-Revision-0

Enabling Grid-Forming Control Under Unbalanced Conditions

Yemi Ojo, Soumyadeep Nag, Temitayo Olayemi Olowu

December 2025

Idaho National Laboratory
Idaho Falls, Idaho 83415

http://www.inl.gov

Prepared for the
U.S. Department of Energy
Under DOE Idaho Operations Office
Contract DE-AC07-05ID14517

Enabling Grid-Forming Control Under Unbalanced Conditions

Yemi Ojo, Soumyadeep Nag, and Temitayo O. Olowu
Department of Power and Energy
Idaho National Laboratory
Idaho Falls, U.S.A.
yemi.ojo@inl.gov, soumyadeep.nag@inl.gov, temitayo.olowu@inl.gov

***Abstract*—Standalone microgrids often experience unbalanced loading and faults, which can cause grid-forming control designed for balanced conditions to produce oscillatory responses. To address this issue, a compact time-domain transformation appropriate for inverter control is proposed, allowing the conversion of unbalanced three-phase signals to positive and negative synchronous reference frames. This transformation supports the development of a grid-forming control with fault ride-through, featuring frequency and voltage droop controllers and nested current and voltage control loops that seamlessly integrate an enhanced current limiter. The effectiveness of the proposed control and transformation is demonstrated through analytical results and electromagnetic transient simulation.**

***Index Terms*—Grid-forming control, unbalanced three-phase signals, unbalanced conditions, standalone microgrids**

I. Introduction

Power grids around the world are experiencing increased penetration of inverter-based resources, which can be deployed as low/medium voltage microgrids. It is projected that 900 GW of electricity will be produced by inverter-based resources by 2031 [1]. Inverter-based microgrids can facilitate local use of variable resources and storage, thereby enhancing flexibility and power quality. Hypothetically, inverter-based microgrids can improve grid resilience by supporting off-grid operations. However, existing inverter control schemes often neglect the imbalances experienced in microgrids. This can hamper large-scale integration of variable resources and storage and realization of reliable independent microgrids. As a result, advanced inverter control are required to ensure microgrid reliability and resilience.

Most inverter-based resources use grid-following strategies that inject predefined active and reactive power but require phase-lock loops to synchronize to the grid [2]. Grid-forming control solves this by providing functions that set and regulate frequency and voltage like synchronous generators. Existing methods include active power-based droop control, angle droop control, and virtual synchronous machine control [3]–[5], which can be integrated with single and nested control loops [3], [4]. The benefits of grid-forming control include the ability to impose self-defined voltage at connection points and enabling independent microgrid operation.

This work is supported through the INL Laboratory Directed Research and Development(LDRD) Program under DOE Idaho Operations Office Contract DE-AC07-05ID14517.

The aforementioned grid-forming strategies assume balanced conditions, which is often not the case in microgrids. Under unbalanced conditions, these schemes produce oscillatory responses due to the inability of the standard Clarke-Park transform to convert unbalanced sinusoids into non-oscillating signals. Few works consider grid-forming control under unbalanced conditions. Some use the proportional resonant controllers in the stationary $\alpha\beta$ reference frame [2], [6], but can perform poorly under large frequency deviations. Others use the double-decoupled synchronous reference frame (DDSRF), but this requires low-pass filters, which cause slow responses [2], [7], [8]. Some can be highly nonlinear and complex [9], [10], with transformations not concisely represented for control design and analysis [2], [7]–[9]. Additionally, power converters cannot replicate the fault response of synchronous generators, necessitating the integration of current limiters in grid-forming control, which have been understudied.

This paper addresses these issues by developing a grid-forming control effective under unbalanced conditions and sets and regulates frequency and voltage, achieves active power sharing, injects negative sequence current, provides voltage support, and limits current during faults. It features frequency and voltage droop controllers and nested current and voltage control loops that nicely integrate with an enhanced current limiter providing fault ride-through. The control design is facilitated through a compact time-domain transformation appropriate for grid-forming control design and eliminates using the use of low-pass filters. The transformation allows the conversion of unbalanced sinusoids into non-oscillatory positive and negative components. Finally, the effectiveness of the proposed control and transformation is demonstrated via a detailed electromagnetic transient (EMT) simulation.

II. A Time-Domain Coordinate Transformation

This section presents a compact time-domain coordinate transformation that is appropriate for grid-forming control design and decomposes unbalanced electrical signals into non-oscillatory positive and negative direct-quadrature (dq) components. To this end, consider a generic three-phase electrical system

$$\dot{x}_{abc}(t) = f(x_{abc}(t)) \tag{1}$$

where $t \geq 0$ and state vector $x_{abc}(t) \in \mathbb{R}^3$ represents unbalanced asymmetric three-phase signals

$$x_{abc}(t) = \sqrt{2}\begin{bmatrix} X_a \sin(\theta(t)+\phi_a) \\ X_b \sin(\theta(t)+\phi_b-\frac{2\pi}{3}) \\ X_c \sin(\theta(t)+\phi_c+\frac{2\pi}{3}) \end{bmatrix}. \tag{2}$$

$\theta(t) \in [0\ 2\pi)$ is the phase angle, $\phi_a \geq 0, \phi_b \geq 0, \phi_c \geq 0$ are constant phase shifts, and $X_a \geq 0, X_b \geq 0, X_c \geq 0$ are the three-phase root mean squared values (RMS), respectively, with $X_a \neq X_b \neq X_c$ and $\phi_a \neq \phi_b \neq \phi_c$. The phase angle, $\theta(t)$, oscillates with frequency $\omega(t) \in \mathbb{R}$, as follows

$$\dot{\theta}(t) = \omega(t). \tag{3}$$

Let $\tau = 1/4f$ where $f = \omega/2\pi$ is the frequency of the unbalanced three-phase signal $x_{abc}(t)$. Then, $x_{abc}(t-\tau)$ denotes the signal $x_{abc}(t)$ delayed by τ[1]. Furthermore, consider the standard Clarke ($\alpha\beta\gamma$) and Park transformation ($dq0$) transformations matrices

$$T_{\alpha\beta\gamma} = \sqrt{\frac{2}{3}}\begin{bmatrix} 1 & -\frac{1}{2} & -\frac{1}{2} \\ 0 & \frac{\sqrt{3}}{2} & -\frac{\sqrt{3}}{2} \\ \frac{1}{\sqrt{2}} & \frac{1}{\sqrt{2}} & \frac{1}{\sqrt{2}} \end{bmatrix}, \tag{4}$$

$$T_{dq0}(\cdot) = \begin{bmatrix} \cos(\cdot) & \sin(\cdot) & 0 \\ -\sin(\cdot) & \cos(\cdot) & 0 \\ 0 & 0 & 1 \end{bmatrix}. \tag{5}$$

A. Employed Coordinate Transformation

To achieve a transformation that is appropriate for grid-forming control, unlike [11], it is oriented such that phase a aligns with the d axis. This is achieved by rotating the $dq0$ transformation matrix (5) clockwise by $\pi/2$, as follows

$$\tilde{T}_{dq0}(\cdot) = T_{dq0}(-\frac{\pi}{2})\, T_{dq0}(\cdot). \tag{6}$$

Therefore, the transformation matrix employed in this paper for the coordinate transformation is given by

$$T(t) = \hat{T}_{dq0}(t) T_{+-0} \hat{T}_{\alpha\beta\gamma} \tag{7}$$

where

$$\hat{T}_{\alpha\beta\gamma} = \begin{bmatrix} T_{\alpha\beta\gamma} & \mathbf{0}_{3\times3} \\ \mathbf{0}_{3\times3} & T_{\alpha\beta\gamma} \end{bmatrix}, \tag{8}$$

$$\hat{T}_{dq0}(t) = \begin{bmatrix} \tilde{T}_{dq0}(\theta(t)) & \mathbf{0}_{3\times3} \\ \mathbf{0}_{3\times3} & \tilde{T}_{dq0}(-\theta(t)) \end{bmatrix}, \tag{9}$$

$$T_{+-0} = \frac{1}{2}\begin{bmatrix} 1 & 0 & 0 & 0 & -1 & 0 \\ 0 & 1 & 0 & 1 & 0 & 0 \\ 0 & 0 & 1 & 0 & 0 & 0 \\ 1 & 0 & 0 & 0 & 1 & 0 \\ 0 & 1 & 0 & -1 & 0 & 0 \\ 0 & 0 & 0 & 0 & 0 & 1 \end{bmatrix}, \tag{10}$$

$T(t), \hat{T}_{\alpha\beta\gamma}, \hat{T}_{dq0}(t), T_{+-0} \in \mathbb{R}^{6\times6}$. and the matrix, T_{+-0}, performs signal cancellation [11]. Then, the time-domain coordinate transformation being employed is given by

$$x^{+-}_{dq0}(t) = \begin{bmatrix} x^{+}_{dq0}(t) \\ x^{-}_{dq0}(t) \end{bmatrix} = T(t)\begin{bmatrix} x_{abc}(t) \\ x_{abc}(t-\tau) \end{bmatrix} \tag{11}$$

[1]A delay of $x_{abc}(t)$ by $\tau = 1/4f$ means a phase delay of $\pi/2$.

where the signals

$$\begin{aligned} x^{+}_{dq0}(t) &= \begin{bmatrix} x^{+}_{d}(t) & x^{+}_{q}(t) & x^{+}_{0}(t) \end{bmatrix}^\top \\ x^{-}_{dq0}(t) &= \begin{bmatrix} x^{-}_{d}(t) & x^{-}_{q}(t) & x^{-}_{0}(t) \end{bmatrix}^\top \end{aligned} \tag{12}$$

denote the $dq0$ positive and negative components which rotate with $\theta(t)$ and $-\theta(t)$, respectively. Noting that T_{+-0} is full rank and $\hat{T}_{\alpha\beta\gamma}$, $\hat{T}_{dq0}(t)$ are orthogonal matrices, then the inverse of matrix, T_{+-0}, exists which is given by

$$T^{-1}(t) = \hat{T}^\top_{\alpha\beta\gamma} T^{-1}_{+-0} \hat{T}^\top_{dq0}(t). \tag{13}$$

Therefore, the inverse coordinate transformation is given by

$$\begin{bmatrix} x_{abc}(t) \\ x_{abc}(t-\tau) \end{bmatrix} = T^{-1}(t)\, x^{+-}_{dq0}(t). \tag{14}$$

Let $\mathcal{K} = \begin{bmatrix} \mathbf{I}_3 & \mathbf{0}_{3\times3} \\ \mathbf{0}_{3\times3} & \mathbf{0}_{3\times3} \end{bmatrix}$, the non-delayed signal, $x_{abc}(t)$, can be recovered by performing

$$x_{abc}(t) = \mathcal{K}\begin{bmatrix} x_{abc}(t) \\ x_{abc}(t-\tau) \end{bmatrix} = \mathcal{K}\, T^{-1}(t)\, x^{+-}_{dq0}(t). \tag{15}$$

Clearly from (7), the employed coordinate transformation in (11) involves three steps. First, the unbalanced signals, $x_{abc}(t), x_{abc}(t-\tau)$, are transformed into the $\alpha\beta\gamma$ components using the standard Clarke transformation (8). This is followed by processing the $\alpha\beta\gamma$ components through the signal cancellation (10), and finally the conversion into the positive and negative $dq0$ components using the $dq0$ transformation (9).

B. Benefit of Employed Coordinate Transformation

To illustrate the advantage of the transformation (7), the explicit expression of the respective components in (11) is obtained as follows (see Appendix A for derivation):

$$x^{+}_{d} = \frac{1}{\sqrt{3}}(X_a \cos\phi_a + X_b \cos\phi_b + X_c \cos\phi_c) \tag{16a}$$

$$x^{+}_{q} = \frac{1}{\sqrt{3}}(X_a \sin\phi_a + X_b \sin\phi_b + X_c \sin\phi_c) \tag{16b}$$

$$\begin{aligned} x^{+}_{0} =& \frac{1}{2\sqrt{6}}[2X_a \sin(\theta(t)+\phi_a) - X_b \sin(\theta(t)+\phi_b) \\ & -X_c \sin(\theta(t)+\phi_c)] + \frac{1}{2\sqrt{2}}[-X_b \cos(\theta(t)+\phi_b) \\ & +X_c \cos(\theta(t)+\phi_c)] \end{aligned} \tag{16c}$$

$$\begin{aligned} x^{-}_{d} =& \frac{1}{2\sqrt{3}}(-2X_a \cos\phi_a + X_b \cos\phi_b + X_c \cos\phi_c) \\ & + \frac{1}{2}(X_b \sin\phi_b - X_c \sin\phi_c) \end{aligned} \tag{16d}$$

$$\begin{aligned} x^{-}_{q} =& \frac{1}{2\sqrt{3}}(2X_a \sin\phi_a - X_b \sin\phi_b - X_c \sin\phi_c) \\ & + \frac{1}{2}(X_b \cos\phi_b - X_c \cos\phi_c) \end{aligned} \tag{16e}$$

$$\begin{aligned} x^{-}_{0} =& \frac{1}{2\sqrt{6}}[-2X_a \cos(\theta(t)+\phi_a) + X_b \cos(\theta(t)+\phi_b) \\ & +X_c \cos(\theta(t)+\phi_c)] + \frac{1}{2\sqrt{2}}[-X_b \sin(\theta(t)+\phi_b) \\ & +X_c \sin(\theta(t)+\phi_c)] \end{aligned} \tag{16f}$$

Evidently, $x_d^+, x_q^+, x_d^-, x_q^-$, are non-oscillatory signals due to constant phase shifts, ϕ_a, ϕ_b, ϕ_c, and RMS values, X_a, X_b, X_c, while x_0^+, x_0^-, oscillate with frequency, ω. This shows the advantage of the coordinate transformation (11) over the standard Park-Clarke transformation, which produces oscillatory dq components under unbalanced conditions. Unlike the DDSRF methods [2], [7], [8], the transformation (11) enables the generation of constant $x_d^+, x_q^+, x_d^-, x_q^-$, thereby eliminating the use of low-pass filters. The same benefit holds if $x_{abc}(t)$ is unbalanced (balanced) and symmetric (asymmetric), i.e., $X_a \neq X_b \neq X_c$ ($X_a = X_b = X_c$) and $\phi_a = \phi_b = \phi_c = \phi$ ($\phi_a \neq \phi_b \neq \phi_c$). The case $X_a = X_b = X_c$, $\phi_a = \phi_b = \phi_c = \phi$, $\phi \geq 0$ shows that the $x_0^+, x_d^-, x_q^-, x_0^-$ in (16) are zero, thus allowing to recover the standard $dq0$ transformation under balanced and symmetric conditions. Note that ϕ_a, ϕ_b, ϕ_c are generally small. Thus, by (16) x_d^+ is considerably larger than x_q^+. This means that the d axis aligns with phase a, a property incorporated into (7) by (6). This is appropriate for grid-forming control where the inverter output voltage (positive) d-component often tracks the desired voltage magnitude [3].

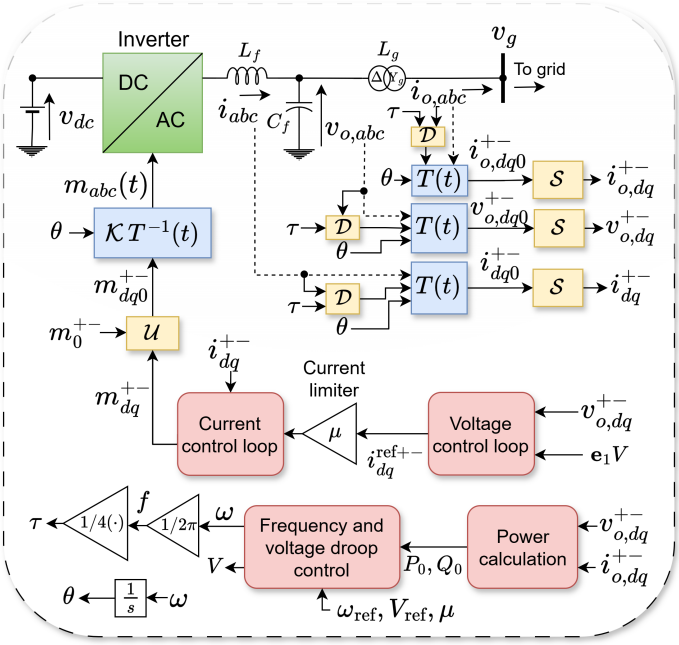

Fig. 1. Inverter with proposed grid-forming control

III. Proposed Grid-Forming Control

Several grid-forming inverters are designed for balanced grids, which means they only inject positive sequence current during unbalanced conditions. However, the recommendations in [12] suggest that grid-forming inverters should also inject negative sequence current and provide fault ride-through during unbalanced conditions. Using the transformation (11), a grid-forming control is proposed to meet these control objectives:

1) Sets and regulates frequency and voltage
2) Shares active power
3) Provides voltage support and injects negative sequence current
4) Provides fault ride-through

These objectives align with the recommendations in [12]. The fourth objective is for grid-forming inverters to respond like synchronous generators during faulty conditions. To this end, the grid-forming control being proposed meets these objectives by featuring a frequency and voltage droop control and nested voltage and current control loops that all nicely integrate an enhanced current limiter.

To proceed, consider the inverter system (Fig. 1) consisting of the inverter circuit, signal transformation, and proposed grid-forming control. The inverter connects to the grid through a Δ-Y$_g$ transformer. The signals, $i_{abc}, i_{o,abc}, v_{o,abc} \in \mathbb{R}^3$, are of the form (2) and are the inverter three-phase input and output currents and output voltage, respectively. $m_{abc} \in \mathbb{R}^3$ is the three-phase modulating signal of the type (2). Since the transformer Δ-winding traps the zero component [9] and power quality improvement is of importance, only the positive and negative components, $i_{dq}^{+-}, v_{o,dq}^{+-}, i_{o,dq}^{+-} \in \mathbb{R}^4$, are used in the control design. To facilitate this, the three-phase signals, $i_{abc}, v_{o,abc}, i_{o,abc}$, are respectively, decomposed into $i_{dq0}^{+-}, v_{o,dq0}^{+-}, i_{o,dq0}^{+-} \in \mathbb{R}^6$ using the coordinate transformation, $T(t)$, in (11). A delay, τ, as in (11) is applied to the delayed block, $\mathcal{D}$ (Fig. 1). Then, $i_{dq}^{+-}, v_{o,dq}^{+-}, i_{o,dq}^{+-}$ are obtained by passing $i_{dq0}^{+-}, v_{o,dq0}^{+-}, i_{o,dq0}^{+-}$ through the signal selectors, $\mathcal{S}$ (Fig. 1). The controllers featured in the grid-forming control are described in Sections III-A–III-C.

A. Frequency and Voltage Droop Control

The aim is to design a frequency and voltage control that sets and regulates both frequency and voltage and shares active power, as specified in the control objectives above. To this end, a frequency and voltage droop control enhanced with a current limiter, $\mu_i > 0$ (designed in Section III-C), is proposed as follows

$$\begin{aligned} \omega_i &= \omega_{\text{ref}} - \mu_i k_{p,i} P_{0,i} \ , \\ V_i &= V_{\text{ref}} - \mu_i k_{q,i} Q_{0,i} \end{aligned} \tag{17}$$

where the subscript, i, indicates inverter i. $k_{p,i}, k_{q,i}$ are the droop gains and ω_i, V_i are the frequency and voltage setpoints. $P_{0,i}, Q_{0,i} \in \mathbb{R}$ are the average (non-oscillatory) active and reactive power and are given by

$$\begin{aligned} P_{0,i} &= v_{\text{odq},i}^{+\top} i_{\text{odq,i}}^{+} + v_{\text{odq},i}^{-\top} i_{\text{odq},i}^{-}, \\ Q_{0,i} &= v_{\text{odq},i}^{+\top} J^\top i_{\text{odq,i}}^{+} + v_{\text{odq},i}^{-\top} J^\top i_{\text{odq},i}^{-} \end{aligned} \tag{18}$$

where $J = \begin{bmatrix} 0 & 1 \\ -1 & 0 \end{bmatrix}$. Using the power, P_0, Q_0, improves power quality and eliminates the use of low-pass filters.

The controller (17) sets and regulates frequency and voltage with appropriate choice of the droop gains, $k_{p,i}, k_{q,i}$. Also, (17) achieves active power sharing. To show this, express (17) for inverters i, j as $\omega_i = \omega_{\text{ref}} - \mu_i k_{p,i} P_{0,i}$ and $\omega_j = \omega_{\text{ref}} - \mu_j k_{p,j} P_{0,j}$. Given that synchronization holds, then $\omega_i^* - \omega_{\text{ref}} = \omega_j^* - \omega_{\text{ref}}$ where ω_i^*, ω_j^* are the equilibrium values of ω_i, ω_j, respectively. This gives $\mu_i k_{p,i} P_{0,i} = \mu_j k_{p,j} P_{0,j}$, which means that active power is shared proportionally.

B. Voltage and Current Control Loops

The goal is to design voltage and frequency control loops that regulate voltage, provide voltage support, and inject negative sequence current, as listed in the control objectives above. Therefore, a nested voltage and current control loop enhanced with current limiter, $\mu \in \mathbb{R}_{>0}$ (designed in Section III-C), is proposed, as follows

$$\begin{aligned} \dot{\eta}^{+-}_{dq,i} &= v^{+-}_{\text{od}q,i} - \mathbf{e_1} V_i \\ i^{\text{ref}+-}_{dq,i} &= -\lambda_P (v^{+-}_{\text{od}q,i} - v^{\text{ref}+-}_{dq,i}) - \lambda_I \eta^{+-}_{dq,i} \end{aligned} \tag{19}$$

$$\begin{aligned} \dot{\zeta}^{+-}_{dq,i} &= i^{+-}_{dq,i} - \mu_i i^{\text{ref}+-}_{dq,i} \\ m^{+-}_{dq,i} &= -C_P (i^{+-}_{dq,i} - \mu_i i^{\text{ref}+-}_{dq,i}) - C_I \zeta^{+-}_{dq,i}. \end{aligned} \tag{20}$$

(19)–(20) describe the voltage and current control loops, respectively, with integrator states, $\eta^{+-}_{dq}, \zeta^{+-}_{dq} \in \mathbb{R}^4$, and proportional $\lambda_{\text{P}}, C_{\text{P}}$ and integral $\lambda_{\text{I}}, C_{\text{I}}$ gains. $i^{\text{ref}+-}_{dq,i}, m^{+-}_{dq,i} \in \mathbb{R}^4$ are the reference current and modulating signal, respectively. Finally, the modulating signal, $m_{abc,i}(t)$, is generated by first augmenting $m^{+-}_{dq,i}$ with the zero components, $m^{+-}_{0,i}$, (chosen as zeros) through a signal augmentation block, $\mathcal{U}$ (Fig. 1) to obtain $m^{+-}_{dq0,i}(t)$. Then, using (15), $m_{abc,i}(t)$ is obtained as

$$m_{abc,i}(t) = \mathcal{K} T^{-1}(t)\, m^{+-}_{dq0,i}(t). \tag{21}$$

The controller (19)–(20) satisfies the control objectives as follows. (19)–(20) ensures that the inverter output voltage tracks the voltage amplitude, $\mathbf{e_1} V_i$. Generating the negative sequence current components in $i^{\text{ref}+-}_{dq,i}$ ensures voltage support and injection of negative sequence current. Providing voltage support entails minimizing $v^{-}_{\text{od}q,i}$ and maximizing $v^{+}_{\text{od}q,i}$, which is achieved by choosing $\mathbf{e_1} = [1\ 0\ 0\ 0]^\top$ in the voltage control loop (19). Ensuring that $v^{-}_{\text{od}q,i}$ tracks $[0\ 0]$ results in the generation of the negative sequence components in $i^{\text{ref}+-}_{dq,i}$, which tracked by $i^{-}_{dq,i}$ in the current control loop (20) ensures that a negative sequence current is injected. Voltage support and negative sequence current injection can be measured using the voltage and current unbalanced factors (VUF, IUF), given by (22) [2].

$$\text{VUF}_i = \frac{\sqrt{v^{-2}_{o,d,i} + v^{-2}_{o,q,i}}}{\sqrt{v^{+2}_{o,d,i} + v^{+2}_{o,q,i}}}, \qquad \text{IUF}_i = \frac{\sqrt{i^{-2}_{d,i} + i^{-2}_{q,i}}}{\sqrt{i^{+2}_{d,i} + i^{+2}_{q,i}}}. \tag{22}$$

C. Current Limiter

The aim is to design an enhanced current limiter that provides fault ride-through, as specified in the control objectives above. This is achieved through the design of μ, as follows

$$\mu_i = \begin{cases} 1 & \text{if } \ \|i^{\text{pk}}_{abc,i}\| \le I_{\text{m}} \\ 1/\sigma & \text{if } \|i^{\text{pk}}_{abc,i}\| \ge \sigma I_{\text{m}}, \quad \sigma > 0; \\ I_{\text{m}}/\|i^{\text{pk}}_{abc,i}\| & \text{if } \ \text{otherwise} \end{cases} \tag{23}$$

where $\|i^{\text{pk}}_{abc,i}\| = \sqrt{2}\max\{i^{\text{rms}}_{abc,i}\}$. I_{m} and σ, respectively, are the threshold current and scaling factor, which can be chosen based on inverter overcurrent ratings. Unlike [6], (23) is enhanced through the use of the lower bound $1/\sigma$ which prevents assigning too small values of $I_{\text{m}}/\|i^{\text{pk}}_{i}\|$ to μ_i during faulty conditions, which can limit the amount of current required to maintain stability.

The current limiter μ provides fault ride-through. To show this, it is well known that small droop gains, k_p, k_q, improve stability [3]. Incorporating μ in (17) ensures that during faulty conditions, the values of $\mu\, k_p$ and $\mu\, k_q$ in (17) are reduced, thereby improving stability. Also, integrating μ in (19)–(20) ensures that the size of $i^{\text{ref}+-}_{dq,i}$ is maintained such that the inverter is protected while riding through faults.

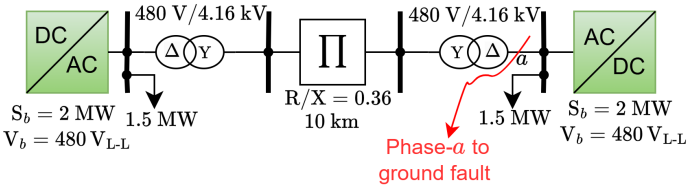

Fig. 2. Two-inverter test system

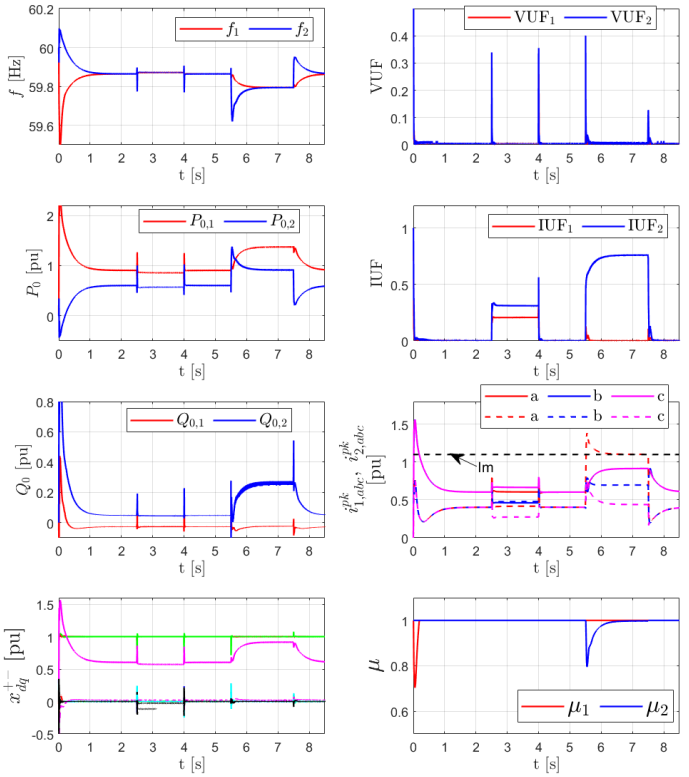

Fig. 3. Test results with $S_{\text{b}} = 2$ MW, $V_{\text{b}} = 480$ $V_{\text{L-L}}$. x^{+-}_{dq} denotes $i^{+-}_{dq,i}, v^{+-}_{o,dq,i}, i^{+-}_{o,dq,i}$ for $i = 1, 2$.

IV. Case Study

The effectiveness of the grid-forming control (17)–(20), (23) is demonstrated through the EMT simulation of a two-inverter system (Fig. 2) with parameters L_f=0.5 mH, C_f=100 μF, ω_{ref}=1 pu, ω_{b}=$2\pi(60)$ rad/s, V_{ref}=1 pu, k_{p1}=2.5×10^{-3}, $k_{p,2}$=$1.5k_{p,1}$, k_q=2.5×10^{-4}, I_{m}=1.1, λ_{P}=20, λ_{I}=800, C_{P}=0.3, C_{I}=20, σ=1.8. The test is performed as follows: balanced loading at 0-2.5 s; unbalanced loading at 2.5-4.0 s; balanced loading at 4.0-5.5 s; a phase-a to ground fault at 5.5-7.5 s; and balanced loading at 7.5-8.5 s.

The signal x_{dq}^{+-} (denoting $i_{dq,i}^{+-}, v_{o,dq,i}^{+-}, i_{o,dq,i}^{+-}$ for $i = 1, 2$) in Fig. 3 confirms that the proposed transformation (14) yields constant positive and negative components at steady state as derived in (16). This is achieved without using low pass filters. Furthermore, the proposed grid-forming control satisfies the control objectives during the unbalanced loading and fault (Fig. 3). The inverters synchronize and active power is shared proportionally ($k_{p,2}/k_{p,1} = 1.5$) despite the unbalanced conditions. Additionally, the grid-forming control provides voltage support (small VUF) and injects negative sequence current (shown by IUF plots). Also, the inverter peak currents, $i_{abc,1}^{pk}, i_{abc,2}^{pk}$, across the three phases are maintained around I_{m} during the fault. Thus, the proposed transformation and control are effective under unbalanced conditions.

V. Conclusion and Future Work

Grid-forming control designed for balanced conditions can produce oscillatory responses under unbalanced conditions. This paper has addressed the problem by presenting a compact time-domain transformation suitable for grid-forming control and converts unbalanced three-phase signals into non-oscillatory positive and negative direct-quadrature components. Using this transformation, a grid-forming control with fault ride-through has been developed. This features frequency and voltage droop controllers and nested current and voltage control loops that all nicely integrate an enhanced current limiter. Analytical and EMT simulations showed that the proposed transformation and grid-forming control are effective under unbalanced conditions. Future work includes (i) comparing the proposed control to existing methods using the standard Park-Clarke transformations, (ii) real-time and experimental validations of the proposed approach on distribution networks, and (iii) examining the interaction of the current limiter with protection systems.

Appendix A
Derivation of Components in (16)

Let s_a=sin$(\theta + \phi_a)$, s_b=sin$(\theta + \phi_b)$, s_c=sin$(\theta + \phi_c)$, c_a=cos$(\theta + \phi_a)$, c_b=cos$(\theta + \phi_b)$, c_c=cos$(\theta + \phi_c)$. Then, using (2), $x_{abc}(t)$ and $x_{abc}(t-\tau)$ become

$$\begin{aligned} x_{abc}(t) &= \sqrt{2}\begin{bmatrix} X_a s_a \\ X_b(-\frac{1}{2}s_b - \frac{\sqrt{3}}{2}c_b) \\ X_c(-\frac{1}{2}s_c + \frac{\sqrt{3}}{2}c_c) \end{bmatrix} \\ x_{abc}(t-\tau) &= \sqrt{2}\begin{bmatrix} X_a \sin(\theta + \phi_a - \frac{\pi}{2}) \\ X_b \sin(\theta + \phi_b - \frac{2\pi}{3} - \frac{\pi}{2}) \\ X_c \sin(\theta + \phi_c + \frac{2\pi}{3} - \frac{\pi}{2}) \end{bmatrix} \\ &= \sqrt{2}\begin{bmatrix} -X_a c_a \\ X_b(\frac{1}{2}c_b - \frac{\sqrt{3}}{2}s_b) \\ X_c(\frac{1}{2}c_c + \frac{\sqrt{3}}{2}s_c) \end{bmatrix}. \end{aligned} \tag{24}$$

Substituting (7) into (11) gives

$$x_{dq0}^{+-}(t) = \hat{T}_{dq0}(t) T_{+-0} \hat{T}_{\alpha\beta\gamma} \begin{bmatrix} x_{abc}(t) \\ x_{abc}(t-\tau) \end{bmatrix}. \tag{25}$$

Equation (25) is solved in steps as follows. Using (8) and (24), then

$$x_{\alpha\beta\gamma}(t,\tau) := \hat{T}_{\alpha\beta\gamma} \begin{bmatrix} x_{abc}(t) \\ x_{abc}(t-\tau) \end{bmatrix} =$$

$$\frac{2}{\sqrt{3}} \begin{bmatrix} X_a s_a + \frac{1}{4}X_b s_b + \frac{\sqrt{3}}{4}X_b c_b + \frac{1}{4}X_c s_c - \frac{\sqrt{3}}{4}X_c c_c \\ -\frac{\sqrt{3}}{4}X_b s_b - \frac{3}{4}X_b c_b + \frac{\sqrt{3}}{4}X_c s_c - \frac{3}{4}X_c c_c \\ \frac{1}{\sqrt{2}}X_a s_a - \frac{1}{2\sqrt{2}}X_b s_b - \frac{\sqrt{3}}{2\sqrt{2}}X_b c_b - \frac{1}{2\sqrt{2}}X_c s_c + \frac{\sqrt{3}}{2\sqrt{2}}X_c c_c \\ -X_a c_a - \frac{1}{4}X_b c_b + \frac{\sqrt{3}}{4}X_b s_b - \frac{1}{4}X_c c_c - \frac{\sqrt{3}}{4}X_c s_c \\ \frac{\sqrt{3}}{4}X_b c_b - \frac{3}{4}X_b s_b - \frac{\sqrt{3}}{4}X_c c_c - \frac{3}{4}X_c s_c \\ -\frac{1}{\sqrt{2}}X_a c_a + \frac{1}{2\sqrt{2}}X_b c_b - \frac{\sqrt{3}}{2\sqrt{2}}X_b s_b + \frac{1}{2\sqrt{2}}X_c c_c + \frac{\sqrt{3}}{2\sqrt{2}}X_c s_c \end{bmatrix} \tag{26}$$

Furthermore, using (10) and (26), then

$$x_{\alpha\beta\gamma}^{+-}(t) := T_{+-0}\, x_{\alpha\beta\gamma}(t,\tau) = \tag{27a}$$

$$\frac{1}{\sqrt{3}} \begin{bmatrix} X_a s_a + X_b s_b + X_c s_c \\ -X_a c_a - X_b c_b - X_c c_c \\ \frac{1}{\sqrt{2}}(X_a s_a - \frac{1}{2}X_b s_b - \frac{1}{2}X_c s_c) + \frac{1}{\sqrt{2}}(-\frac{\sqrt{3}}{2}X_b c_b + \frac{\sqrt{3}}{2}X_c c_c) \\ X_a s_a - \frac{1}{2}X_b s_b - \frac{1}{2}X_c s_c + \frac{3}{2}X_b c_b - \frac{3}{2}X_c c_c \\ -\frac{3}{2}X_b s_b + \frac{\sqrt{3}}{2}X_c s_c + X_a c_a - \frac{1}{2}X_b c_b - \frac{1}{2}X_c c_c \\ \frac{1}{\sqrt{2}}(-\frac{\sqrt{3}}{2}X_b s_b + \frac{\sqrt{3}}{2}X_c s_c) + \frac{1}{\sqrt{2}}(-X_a c_a + \frac{1}{2}X_b c_b + \frac{1}{2}X_c c_c) \end{bmatrix} \tag{27b}$$

Finally, using (9) and (27), performing $x_{dq0}^{+-}(t) = \hat{T}_{dq0}(t) x_{\alpha\beta\gamma}^{+-}(t)$ yields (16).

References

[1] North American Electric Reliability Corporation. (2022) Inverter-based resource strategy - ensuring reliability of the bulk power system with increased levels of bps-connected ibrs. [Accessed 05-22-2025]. [Online]. Available: https://https://www.nerc.com/comm/Documents/NERC-IBR-Strategy.pdf

[2] R. Teodorescu, M. Liserre, and P. Rodriguez, *Grid converters for photovoltaic and wind power systems*. John Wiley & Sons, 2011.

[3] N. Pogaku, M. Prodanovic, and T. C. Green, "Modeling, analysis and testing of autonomous operation of an inverter-based microgrid," *IEEE Transactions on Power Electronics*, vol. 22, no. 2, pp. 613–625, 2007.

[4] Y. Ojo and K. Laib, "A decentralized polytopic control design for a nonlinear grid-forming inverter model," *IEEE Transactions on Control of Network Systems*, 2024.

[5] Y. Li, Y. Gu, and T. C. Green, "Revisiting grid-forming and grid-following inverters: A duality theory," *IEEE Transactions on Power Systems*, vol. 37, no. 6, pp. 4541–4554, 2022.

[6] N. Baeckeland, D. Venkatramanan, M. Kleemann, and S. Dhople, "Stationary-frame grid-forming inverter control architectures for unbalanced fault-current limiting," *IEEE Transactions on Energy Conversion*, vol. 37, no. 4, pp. 2813–2825, 2022.

[7] M. Reyes, P. Rodriguez, S. Vazquez, A. Luna, R. Teodorescu, and J. M. Carrasco, "Enhanced decoupled double synchronous reference frame current controller for unbalanced grid-voltage conditions," *IEEE Transactions on power electronics*, vol. 27, no. 9, pp. 3934–3943, 2012.

[8] M. Reyes, P. Rodríguez, S. Vázquez, A. Luna, J. M. Carrasco, and R. Teodorescu, "Decoupled double synchronous reference frame current controller for unbalanced grid voltage conditions," in *2012 IEEE Energy Conversion Congress and Exposition (ECCE)*. IEEE, 2012, pp. 4676–4682.

[9] M. Awal, M. R. K. Rachi, H. Yu, I. Husain, and S. Lukic, "Double synchronous unified virtual oscillator control for asymmetrical fault ride-through in grid-forming voltage source converters," *IEEE Transactions on Power Electronics*, vol. 38, no. 6, pp. 6759–6763, 2022.

[10] A. G. Paspatis and G. C. Konstantopoulos, "Voltage support under grid faults with inherent current limitation for three-phase droop-controlled inverters," *Energies*, vol. 12, no. 6, p. 997, 2019.

[11] Y. Ojo and J. Schiffer, "Towards a time-domain modeling framework for small-signal analysis of unbalanced microgrids," in *2017 IEEE Manchester PowerTech*. IEEE, 2017, pp. 1–6.

[12] B. Kroposki, "UNIFI specifications for grid-forming inverter-based resources (v. 2)," National Renewable Energy Laboratory (NREL), Golden, CO (United States), Tech. Rep., 2024.